February 28, 2001, FTM2001-03, Version 3.2

A Proposal For Additional Photometric Bands

Astrometric And Photometric Accuracies

Rob Olling

USNO/USRA, Washington, DC

ABSTRACT

The effectiveness of a 4-band SDSS photometric system and alternative 8-band systems are compared. The 8-band filter system is chosen so as to measure astrophysically important lines and features such as the line-blanketing, Hβ, Mg b, Na D, TiO, the Paschen jump, and the NIR CaII triplet. A preliminary attempt has been made to optimize the central wavelengths and bandwidths ($\sim$ 100 nm) for astrophysical return (narrow bands) and accuracy (wide bands).

Photometry in the 8-band system would be about 10 mmag (5.1 mmag for SDSS), but still good enough to determine stellar temperatures and extinction to 1-6% (T_{eff} to 3%, A_V to $\pm$60 mmag, and R_V to 1.5%) **at V=15**. The analysis technique is rather unsophisticated and can be improved upon. The surface-gravity accuracy is sufficient to perform good luminosity determination (0.3-0.6 dex). The metallicity accuracy is moderate (0.3-1.0 dex) but sufficient for dwarf-subdwarf separation ($\delta[Fe/H] \sim 1.5$). These results are about twice worse than those obtained by Bailer-Jones (2000) for the 11-band GAIA system.

The proposed Mgb filter has a similar transmittance as the neutral-density filters for V=7-9 stars, and can be used instead of this ND filter. Likewise, the narrowest filter proposed has a bandwidth of only 30 nm, so that it could act as a neutral-density filter for the brightest stars ($5 < V < 7$). This would: 1) reduce the photometric errors in the other bands, 2) increase the number of near-simultaneous photometric observations, 3) achieve virtually color-independent astrometry for bright stars.

To first order, it follows that the astrometric accuracy is proportional to $FWHM_{PSF}^{3/2}$ and that the photometric errors are independent of the width of the point-spread function.

1. Introduction

For many astro-physical problems to be addressed by FAME, the astrometry will be of such quality that astrometry will not be the limiting factor in the analysis. Such a situation has never occurred before in astronomy. This slight changes to the current FAME photometric proposal are meant to remedy that situation.

Obviously, at least five color[1] measurements are required so as to determine the five parameters that determine observable stellar spectra to good approximation: T_{eff}, $log(g)$, $[Fe/H]$ and the two parameters describing the interstellar extinction: A_V, R_V. If any of the other physical parameters need be determined, more bands are needed For example, the proposed 8-band system might also be able to determine the α-element enhancement (as GAIA is designed to do).

The GAIA mission has the specific goal to study the "Composition, Formation and Evolution of the Galaxy." It will accomplish this goal employing an intermediate-band photometric system that allows for a 3D classification of the 1 billion GAIA target stars (and a detailed map of the Galactic extinction field). The composition, formation and evolution of the Milky Way can be studied once the ages of stars have been determined. The aim of this document is to show that the FAME mission can achieve a significant part of GAIA's science goals by implementing an extension of FAME's SDSS photometric system.

Stellar evolution models show that as stars evolve, the observable consequences are: 1) larger radii, 2) larger luminosities, 3) lower surface gravities, and 4) different surface temperatures. Traditionally, the effects of surface temperature and gravity on stellar spectra have been used to infer stellar ages. After all, the other two observables (radii and luminosities) depend critically on stellar distances, which are currently poorly known. With GAIA and FAME *and accurate extinction measurements*, the luminosity method can be applied to stars that are close enough for a reliable distance determination. The temperature-gravity method should be used for the more distant stars for which the photometric gravity determination is more reliable. For example, the Sun has brightened by a factor of approximately two during the last 5 billion years. Thus, for a Solar-type star, a 10% distance error corresponds to a 20% luminosity uncertainty and hence a 1 Gyr age uncertainty for a contemporary of the Sun.

[1]Obtained from six photometric bands.

1.1. 3D Classification of Stars

Narrow-band photometric systems such as DDO (McClure & van den Bergh 1968) or intermediate band photometric systems such as the Strömgren (Jordi *et al.* 1997) or Vilnius (Straižys & Sviderskiene 1972) systems can be used for three-dimensional classification of most stars. The three fundamental stellar properties that determine stellar spectra are: 1) effective temperature (T_{eff}), 2) surface gravity [$log(g)$] and 3) metallicity (i.e., the iron abundance, [Fe/H]). In addition, parameters such as the α-elements abundance enhancement, micro-turbulent velocity and the projected rotation speed play a role (for a minority of stars). These stellar parameters are listed in order of "ease of determination:" T_{eff} is easiest, luminosity-class [$log(g)$] comes second and metallicity is not so easy employing intermediate band photometry. Note that the very hottest stars ($T_{eff} \geq 30,000$ K) have hardly any spectral features, so that neither surface gravity nor metallicity can be determined well. In fact, this very property makes these hot stars with "featureless spectra" suitable to determine the extinction law.

All these parameters are best determined from high-resolution and high signal-to-noise spectra. However, it is well known that a "reasonable" three-dimensional classification can be accomplished for most stars using, for example, the Strömgren or Vilnius photometric systems. The Vilnius photometric system can do: $\pm$0.2 dex in metallicity, $\pm$0.5 mag in absolute luminosity and $\pm$0.03 mag in extinction, for 2 mmag photometry. However, with the Vilnius bands of $\Delta\lambda \sim 26$ nm FAME will reach approximately ten times worse (17 mmag) photometric accuracies, and comparably worse for surface temperature and extinction. Furthermore, the Vilnius system has 2-3 bands that are too blue for the FAME passband. Similar accuracies, bandwidths and attainable accuracies hold for the Strömgren system.

In a recent paper, Bailer-Jones (2000) investigated how well a photometric system comprising a mix of broad-band and intermediate-band filters can be used for the 3D classification of stars, as well as the determination of interstellar extinction. His simulations show that such 10 to 15 band photometric system can measure "T_{eff} to 1% and [Fe/H] to $\pm$0.2 dex across a large range of temperatures (4,000 -30,000 K) and metallicity (-3 to +1 dex), and $log(g)$ to $\pm$0.2 dex for stars earlier than solar" at high signal-to-noise ratios (S/N ≥ 50, or $\delta m \lesssim 0.02$ mag). Such photometric accuracy will be well improved upon by FAME, but unfortunately in only four bands, in the current design. On the other hand, the current FAME design does not contain "UV" filters, so that neither the Balmer jump around 365 nm nor the line-blanketing effects are included in the FAME data. As a result, FAME's determinations of metallicity will be less accurate.

1.2. Interstellar Extinction

Interstellar extinction fades and reddens the intrinsic stellar spectra. However, extinction in the optical region is mostly "featureless," so that two parameters suffice to characterize the wavelength dependence of interstellar extinction. Cardelli, Clayton & Mathis (1989) determined that the extinction at wavelength λ is given by:

$$A(\lambda) \;=\; A(V) \times [a(x) + b(x)/R_V] \tag{1}$$

where $A(V)$ is the extinction in the Johnson V band, R_V the ratio of selective to total extinction and $a(x)$ and $b(x)$ are polynomials in $1/\lambda$. In the Milky Way, the R_V value is known to vary by tens of percent, where its value seems to depend on the average density of the interstellar medium, with a typical value of $R_V \sim 3.1$. The extinction law of eqn. (1) is presented in figure 1. If stellar temperatures and interstellar extinction are to be accurately determined, it is clear from figure 1 that the R_V parameter needs to be determined from spectra as well. If the R_V value is *assumed* rather than determined, a relative benign variation of R_V of 0.5 (16%) results in a 10% bias in the inferred extinction. My experiments also indicate that such R_V bias leads to temperature dependent biases in the inferred T_{eff} and $log(g)$ and to a doubling of the scatter in the T_{eff}, A_V and $log(g)$ determinations.

Such extinction biases would have unacceptable consequences for the absolute luminosity calibration of, for example, Cepheids whose median extinction is about 1.5 magnitudes[2].

1.3. Outline

In section 2, I present a possible photometric scheme that can be implemented in the FAME mission so that a "reasonable" 3D classification of stars can be obtained for the majority of FAME targets. A consequence of better photometric parameterization of stars is also a better modeling of the color-dependent effects in the derivation of the astrometric parameters. On the other hand, more bands lead to more calibration parameters and fewer observations per band.

In section 2.1, I discuss some of the practical consequences of using 8 rather than four filters. In section 3, I perform an error analysis for astrometric (§ 3.1) and photometric (§ 3.2) errors. When systematic errors are neglected, it follows that the astrometric accuracy is proportional to $FWHM_{PSF}^{3/2}$ and that the photometric errors are independent of the width of the point-spread function. In section 4, I present the results of the currently employed scheme to perform a 3D classification of stellar spectra and the determination of

[2]For the closest 200 or so Cepheids.

interstellar extinction. In section 5 I find that the Mg2 and TiO_C filters are viable and sensible alternatives to neutral-density filters. Section 6 sums up.

2. Alternative Filter Choices

I propose to employ an 8-band filter system for FAME (see table 1 and/or figure 2). This system is in part inspired by GAIA's choices, in part by the desire to have an overlap with the SDSS system, as well as by filter-width considerations. However, this particular choice of filters is by no means very sophisticated and can most likely be improved upon. Furthermore, the current analysis of the achievable accuracies is preliminary and not entirely satisfactory. GAIA uses 11 intermediate and narrow band filters. From GAIA's 11 filter we reach the FAMEous 8 in the following way: 1) we drop their narrow Hα filter (F65N, $\delta\lambda$ =5 nm), 2) we employ only one of their two TiO $\sim$30 nm indices, and 3) drop the reddest filter.

The properties of the proposed 8-band FAME filter set are summarized in table 1. The average bandwidth of these filters is about 100 nm, or 77% of the width of the SDSS filters. I propose to retain the SDSS g', r' and i' filters, but drop the z' filter. However, SDSS u' will be included as well as three specialized filters: 1) a "line-blanketing" filter at 422 nm, 2) a MgH filter at 520 nm, and 3) a 875 nm band centered on the near-infrared CaII triplet. Further motivation for these choices is given in the following subsections. I also propose to assign somewhat larger covering fractions (F_{CCD}) to the filters with narrower bands so as to obtain more transits and hence more similar photometric accuracies for all bands at the end of the mission. However, in order to retain a minimum of 25 transits during the 2.5 years mission, F_{CCD} has to exceed 0.35.

2.1. Some Practical Consequences

The current design of FAME's photometric CCDs is redundant: each of the 4 SDSS filters is implemented on two different CCDs. Redundancy will also be part of the 8 band system. This means that each CCD will be covered by 3 or 4 filters. Hugh Harris reports that about 7.5% of the CCD area will be covered with filter-glue if 4 filters are used per CCD. This would reduce the number of transits/observations by 7.5% as well and a loss of photometric accuracy of 3.75% with respect to the ideal, no-loss, case.

Current estimates of the number of transits for 14 astrometric CCDs are of order 1060, or 75.7 transits per CCD. For 8 filters on 4 CCDs, this would translate into approximately 37.8 transits per filter. However, in the ecliptic region with $|\sin(\beta)| \lesssim 0.25$, about one-third of the stars will be seen only half as many times. With a minimum area of 0.35 CCDs, the vast majority of stars will have $\gtrsim 25$ photometric measurements during the 2.5 year mission.

Table 1: Properties of the 8-band (top part) and SDSS (lower part) filter systems. The band designations, central wavelengths FWHM and system throughput are listed in the first four columns. The 5^{th} column gives the 2.5yr-mission photometric accuracy scaled to a 5 mmag error for an average SDSS filter, *assuming unity throughput and 1 CCD*. The achievable mission-end precision is tabulated in #6. These numbers include the actual throughput (#4) and CCD covering fraction (#7). The mission-end number of observations per filter is listed in #8. The values in brackets in the last three columns are for the case that the TiO-continuum filter is used for bright-star astrometry. The average mission-end photometric precision is 12.1 mmag (10.6 if the TiO_C band is used for bright-star astrometry). On average, the 8-band system has errors 142% (100%) worse than the 4-band SDSS system.

filter name (1)	λ_0 [nm] (2)	$FWHM$ [nm] (3)	$< TP >$ (4)	δm_1 [mmag] (5)	δm_M [mmag] (6)	F_{CCD} (7)	N_{obs} (8)
u'	352.0	63.0	0.14	6.50	17.2 (17.2)	1.00 (1.00)	71.4 (71.4)
F422	422.5	75.0	0.61	5.96	12.9 (10.6)	0.35 (0.52)	25.0 (37.2)
g'	480.0	141.0	0.76	4.35	8.4 (8.4)	0.35 (0.35)	25.0 (25.0)
Mg b	520.0	50.0	0.83	7.30	13.6 (10.6)	0.35 (0.57)	25.0 (40.8)
r'	625.0	139.0	0.83	4.38	8.2 (8.1)	0.35 (0.35)	25.0 (25.0)
i'	769.0	154.0	0.68	4.16	8.5 (8.5)	0.35 (0.35)	25.0 (25.0)
TiO_C	745.0	30.0	0.73	9.42	14.0 (6.4)	0.62 (3.00)	44.2 (214.0)
Ca II	875.0	85.0	0.45	5.60	14.0 (10.6)	0.35 (0.62)	25.0 (44.5)
g'	480.0	141.0	0.76	4.35	5.00	0.99	70.9
r'	625.0	139.0	0.83	4.38	5.00	0.92	66.0
i'	769.0	154.0	0.68	4.16	5.00	1.01	72.1
z'	911.0	141.0	0.32	4.35	7.78	0.98	69.7

The periods of many variable stars (e.g. Cepheids) depend on color. In fact, the surface gravity and effective temperature depend significantly on the pulsation phase, especially for the important long-period Cepheids (Fry & Carney 1997). Thus, photometric simultaneity is desirable, and we should optimize the filters-locations on the CCDs to achieve this goal. For each focal plane transit, two photometric CCDs will be traversed to yield two observations 4.7 seconds apart. When the same star is observed by the second viewport, 9 minutes later, the cross-scan position of the star has changed by 519 $\pm$375 pixels. With an allocation of 512 pixels/filter (4 filters per CCD), chances are that a photometric datum in another filter is obtained. Thus, with the appropriate layout of filters on the photometric CCDs, there is a reasonable chance that photometry is "simultaneous" in 4 bands (+ the astrometric band).

Alternatively, one could conceive of a situation in which the photometric filters are

rotated with respect to the scan direction. In this case, these CCDs need be read out in start-stop mode, in such a manner that each "start" corresponds to a different filter.

2.2. Metallicity Determination

The broad and intermediate-band systems discussed above all share a common feature that the overall metallicity is measured by the line-blanketing effects red-wards of 400 nm. I propose a "line-blanketing band" centered at 422.5 nm (F422) with a full-width at half maximum (FWHM[3]) of 75 nm. The 1/4-width of this bands extends to 381 nm, but not as far as the absorption feature induced by the silver mirror-coatings at approximately 370 nm.

Other "metal" lines are measured in the 8-band system: the Mg b, Na D, and Ca II are located in the F530, F625 and F875 bands. Further TiO can be determined from the i' and TiO_C bands. However, most of these lines are also sensitive to surface-gravity variations, and often more strongly so. As a result, the "3^{rd}" stellar classification parameter (metallicity) is least well determined in the proposed 8-band system. It should be noted that Mg b, Ca II and TiO measure the α-element abundance. Thus, in principle, it is possible to determine the α-element enhancement from the F422-line-blanketing flux and the α-element indices. Further note that since iron lines are prevalent in all parts of the spectrum, metallicity has some effect on all bandpasses.

2.3. Surface Gravity Determination

The primary $log(g)$ indicator –the Balmer jump– is located rather far into the blue, where the overall throughput of the optics is only about 14%. As a result, the magnitude errors in the u' band will be two to fourteen times[4] larger than in the Johnson V band.

I propose to determine surface gravity of hot stars by three means: a) via the Balmer jump (u'-F422), b) via the F422 Balmer decrement (F422-g')[5], and c) the Paschen jump at 820 nm (i'-F875).

In intermediate and late-type stars, the Mgb index around 520 nm and the near-IR C II

---

[3]For computational convenience, I use bandpasses of the following form: $T(\lambda) = \exp\left(-\frac{1}{2}((\lambda - \lambda_0)/\sigma)^8\right)$, with $\sigma = 1.135 \times FWHM/2.3548$. This functional form has steeper edges than a "Gaussian" bandpass, but not as steep as a pill-box function. The full-width at 3/4 (1/4) maximum is 10% smaller (larger) than the $FWHM$.

[4]Factor 2 at 30,000K, factor 4 at 8,000K, factor 7 at 5,000K.

[5]In fact only Hγ, Hδ and Hϵ fall in this band.

triplet near 860 nm are very much sensitive to surface gravity. To ensure a good measurement of these indices, continuum need to be measured. The g' and r' bands are available for the Mgb feature. The continuum of the CaII-triplet band (F875) band is set by the i' band. Also note that since pressure broadening affects all lines, surface-gravity has some effect on all bandpasses.

2.4. Temperature and Extinction Determination

The SDSS g' (F480), r' (F625) and i' (F769) [and the F965] bands are located in parts of the spectrum that are rather free of lines in stars with temperature larger than about 4,500 K. These bands are thus most useful to define the overall shape of the stellar spectrum (i.e., effective temperature and interstellar extinction).

3. Astrometric And Photometric Accuracies

Astrometric and photometric accuracy are intimately linked by the algorithm that is used to perform the analysis. I illustrate this with the example of a purely Gaussian point-spread function (PSF). Similar arguments are valid for different, symmetric PSFs, while the case of asymmetric PSF requires special treatment. Systematic effects such as electron traps, cosmic-ray events, inter-pixel gaps, sensitivity variations and residual flat-fielding problems are neglected. With these simplifications, I find that the astrometric accuracy is proportional to the in-scan PSF width to the 3/2 power. The photometric accuracy is not affected by in-scan smearing.

3.1. Astrometric Accuracy

A detailed treatment of the statistics of the detection experiment shows that the centroiding accuracy (δx_0) is given by:

$$\delta x_0 \quad = \quad \alpha \frac{\lambda}{\pi D} \frac{1}{S/N} \tag{2}$$

where λ, D and S/N are the wavelength, telescope diameter and signal-to-noise ratio. The α parameter depends on "... system geometry, sampling resolution, detector noise, pixel size, ..." (e.g., GAIA, page 253, eqn.30). Similar results have been obtained elsewhere (e.g., Reasenberg, TM96-04). In my simulations of FAME-like Gaussian PSF I find:

$$\delta x_0 \quad \sim \quad 0.857 \, \frac{\sigma_{PSF,pix}}{S_{max}/N} \quad [pixels] \tag{3}$$

where $\sigma_{PSF,pix}$ (in units of pixels) and S_{max}/N are the dispersion and the peak signal-to-noise ratio of the Gaussian. For example, if the effective in-scan and cross-scan full-width at

half-maximum (FWHM[6]) equal $\sqrt{2}$ and $4\sqrt{2}$ pixels, a V=9 star would yield 950k electrons, a 602k electrons peak flux in the marginalized (1D) distribution and a peak signal-to-noise ratio of 775. As a result, the single-observation astrometric accuracy would be 0.133 mas, about 4.4 times better than the nominal mission requirements of $1/350^{th}$ of a pixel.

Following Monet and Zacharias, I again have to stress the importance of keeping the in-scan PSF as narrow as possible. From equation 3 it follows that an *increase* of the PSF has *two* effects: 1) the flux will be distributed over more pixels so that S_{max}/N decreases, and 2) σ_{PSF} increases. For a Gaussian, the total flux follows from the peak signal: $F = \sqrt{2\pi}\,\sigma_{PSF,pix}\,S$. Thus, for constant total flux, the centroiding accuracy is given by:

$$\frac{\delta x_0}{0.857} \sim \frac{\sigma_{PSF,pix}}{(S/N)} = \frac{\sigma_{PSF,pix}}{\sqrt{S}} = \sqrt{\frac{\sqrt{2\pi}}{F}}\,\sigma^{3/2}_{PSF,pix} \quad [pixels] \tag{4}$$

Thus, increasing the PSF at constant flux is proportional to three-half power of the PSF width. The poly-chromatic rms-width of an A0V star is about 0.25 pixels. Since I assumed an "in-scan smearing" with $\sigma_{smear} = 0.55$ pixels, the final PSF is substantially wider than the "optical" PSF ($\sigma_{TOT} = 0.6$ pixels). Equation 4 predicts that if the in-scan PSF were smeared by an additional 0.6 pixels rms, the centroiding accuracy would be $\sqrt{2}^{3/2} \sim 1.7$ times worse. This behavior is confirmed by Monte-Carlo simulations.

For more realistic PSFs that include wings or asymmetries, the numerical pre-factor in equation 3 changes, but the over all width dependence remains the same. Read-noise and digitization effects have virtually no influence on these results.

3.2. Photometric Accuracy

The situation is much more favorable for the attainable *relative* photometric accuracy. The basic reason for this is that the total flux in a 1D image is much better determined than either the centroid, the peak flux or the width of the distribution: flux-determination algorithms in essence add photons and shouldn't care as to how the flux is distributed among the pixels.

Absolute photometry is much more difficult. For example, a certain fraction of the light will fall outside the downlink-windows (Zacharias, FTM2000-21). This fraction depends on, among others, the cross-scan smear, the in-scan and cross-scan positioning errors, the effective wavelength of the star and the location of the CCD in the focal plane. All these effects will have to be calibrated and corrected for.

---

[6]For a Gaussian, $FWHM \sim 2.3548\sigma$.

Using the same simulations and model parameters as for the centroiding experiments described above, Monte-Carlo experiments indeed confirm that **the photometric accuracy is independent of the width of the PSF,** where the photometric errors are given by the square-root of the **total** number of photons. I summarize the results in tables 2-4 below. These tables report astrometric and photometric results for the astrometric CCDs ($\Delta\lambda = 563$ nm), the SDSS filter set ($\Delta\lambda = 130$ nm) and an 8-band filter system with narrower bands ($\Delta\lambda = 65$ nm) than I propose for FAME. These tables were calculated employing photon statistics (and digitization and noise) and assume 1060 observations for the 14 astrometric chips. The number of electrons for the photometric chips were scaled as $(\frac{\Delta\lambda}{563})$, while the number of observations equals $75.7 \times 4/N_{bands}$ for the SDSS and this particular 8-band systems.

Inspecting these tables, we see that very good photometry can be obtained in the photon-statistics limit. In the 8-band photometric system of table 4, the mission-wide magnitude error for 15^{th} magnitude stars are about 10.8 mmag. Thus, even in this case, the worst signal-to-noise ratio (92.6) exceeds the value (50) identified by Bailer-Jones as critical for sufficient 3D classification of stars. The actual 8-band system proposed (table 1) has an average bandwidth of 100 nm and falls between the 130-nm SDSS and the 65-nm systems.

Note that the GAIA report follows a similar procedure to estimate astrometric and photometric errors, but they also include an addition 20% increase to account for other systematic effects such as inter-pixel gap et cetera. Further, it is worth noting that the photometry is likely to be less affected by unmodeled systematics than the centroiding results. After all, for centroiding it is of crucial importance to know where exactly the photons landed. On the other hand, for photometry, it is important that the photons *be counted* while it is less important to know their locations.

4. Current 3D Classification Of Stellar Spectra

Many methods have been used to determine the spectral type, luminosity class and metallicity of stars. Of course, these methods have to be calibrated. Currently I use a library of (15,937) model-atmospheres that have been used to calculate emergent spectra at 2 nm resolution (Le Jeune, Cuisinier & Buser 1997). These models[7] cover a wide range in T_{eff}, $log(g)$ and $[Fe/H]$ and can thus be used to test classification methods. A comparison of models with different parameters requires that model spectra are normalized internally at

[7]I discovered some problems with the published models at certain gravities and metallicities. I deleted some and re-determined others via interpolation. Also note that these models do not vary [α/Fe], and are for a given micro-turbulent velocity.

a given wavelength/band. I choose to normalize the spectra in the Johnson V band.

In practice it may be better to use spectral energy distributions (SEDs) of *real* stars as models never quite capture all the finesse of actual astrophysical objects. This would require a library of stars will well determined T_{eff}, $log(g)$ and $[Fe/H]$ values: the same set of stars that is used to calibrate the stellar atmosphere models. In either case, the classification results will only be as good as the library of input "spectra." Special care needs to be taken to classify outliers.

It is instructive to see some of the spectral diversity that we are trying to measure. In figures 3-5 I present three sets of spectra at $T_{eff} = 10000, 5500$ and 3500 K. In each figure, the left-hand set is for $[Fe/H]$ =-2, the right-hand set for $[Fe/H]$ =-0.5. The plotted spectra (top panels) are for various surface gravities. From these spectra it is apparent that $log(g)$ variations are relatively large. Magnitudes are determined by integrating the SEDs over the bandpasses while they are normalized to the i' band. The results are plotted in the middle panels. In these plots, all $log(g)$ models have seemingly identical magnitudes. The $log(g)$ variations become apparent only when subtracting an average magnitude in each band (bottom panels). Note that the variations seen in the SDSS bands (squares) are very similar to the variations in the narrower bands (crosses).

Metallicity dependent color variations are more subtle. The metallicity variations are better visualized by plotting the colors as a function of metallicity at fixed temperature and surface gravity. I present and example for early G-type stars in the left-hand panel of figure 6. Here it is clear that, as stated in section 2.2, the blue bands exhibit the largest metallicity variation (line-blanketing). The trends become stronger (weaker) for the cooler (hotter) stars.

4.1. Magnitude Error Determinations

At this point I will explain how I determine expected errors in a given band. In table 1 I listed errors of about 10.5 mmag for each band. However, this error depends on the flux distribution of the star and the response of the optics-ccd-filter system. For classification purposes (see below) it is important to take these effects fully into account.

Errors are determined in a four-step process: 1), I determine the number of *photons* in each band with the assumption that ∼46,936 photons ($\delta m \sim 5$ mmag) are detected in the Johnson V band, for a filter that uses 1 photometric CCD. In the right-hand panel of figure 6, I plot the results for the filter set tabulated in table 1. Notice the strong T_{eff} dependence of the errors, especially in the u' band. 2) I scale the errors by the number of

CCDs that are assigned to each band[8]. 3) I scale the errors such that the average of the g', r' and i' bands have δm=5. Finally, since the ∼46,936 photons in V correspond to V=15, I scale to the desired apparent magnitude.

4.2. Practical 3D Classification Schemes

4.2.1. Extinction-free Indices

A method that has been widely used by, for example, the Strömgren and Vilnius groups is that of extinction free indices. In the Strömgren system, the $[m_1]$ and $[c_1]$ indices are good temperature and metallicity indicators for stars of a given surface gravity. Reddening-free indices (Qs) can be determined from magnitudes in any three bands a, b, c (e.g. Mihalas & Binney 1981):

$$Q_{abc} = (m_a - m_b) - \frac{E_{a-b}}{E_{b-c}}(m_b - m_c) = (m_a - m_b) - \frac{A_a - A_b}{A_b - A_c}\,(m_b - m_c) \qquad (5)$$

$$Q_{UBV} = (U - B) - \frac{E_{U-B}}{E_{B-V}}(B - V) = (U - B) - \frac{\frac{A_U}{A_V} - \frac{A_B}{A_V}}{\frac{A_B}{A_V} - 1}\,(B - V)\ , \qquad (6)$$

where E_{a-b} is the color excess for bands a and b, and A_a the extinction in band a with $A_a = R_V E_{a-V}$. The Johnson Q_{UBV} parameter (eqn. [6]) is presented as an example and has been widely used to classify hot stars. The extinction *ratios* can be determined from equation (1) above, and depend only on the assumed R_V value. The value of the $\frac{A_a - A_b}{A_b - A_c}$ factor ranges between 0.2 and 20. As a result, the errors in certain Q's will be relatively small or very large, respectively.

For example, a $Q_{F423,F625,F875} - Q_{F530,F769,F965}$ diagram (not shown) for T_{eff} =6000 K substantiates the classifying power of $Q - Q$ diagrams as gravity and metallicity effects separate nicely at the level of our expected errors: classification errors of order 0.2-0.6 dex are expected at 6,000 K. Further, the size of the classification errors depends on metallicity and $log(g)$. Typically, these $Q - Q$ classification schemes work best for limited ranges of temperature, gravity or metallicity. I found some $Q - Q$ combinations that do a reasonable job (±0.6 dex) at 3D classification when working with four different temperature ranges.

---

[8]The CCD-area assignment is determined from several conflicting requirements: 1) the desire to assign larger areas to those filters that have smallest throughput (u' & F875), 2) a certain minimum number of detector area (0.35) so as to ensure a minimum number of mission-end transits, and 3) a certain maximum CCD area (1.0) to make sure that not all photometric CCDs end up having u' filters (as "required" by condition 1). An example of such CCD-area assignment is tabulated in table 1, as well as the effects on the expected magnitude errors (for an object that has a constant number of photons per unit wavelength).

In principle, it proves useful to use *more* Q_{abc}'s as each is sensitive to a different (non-linear) combination of T_{eff}, $log(g)$ and $[Fe/H]$. I investigated the limit of this approach by employing *all* Q's. I define a $N_Q = 56$-dimensional vector $\overline{Q} = (Q_{1,2,3}, Q_{1,2,4}, Q_{1,2,5}, ...Q_{6,7,8})^T$ for each of the 16k model atmospheres i. This is the training set of models. Test models j that need to be classified are selected from the training set and perturbed by the appropriate amount of noise for a V=15 star (5 mmag for the SDSS filters, 10.5 mmag for the 8-band system). The test and training spectra are compared by computing the error-normalized distance between "observation" and model:

$$\chi^2_Q(j) \;=\; \Delta||\overline{Q}(j)|| = \sum_{i=1}^{i=15,937} \sum_{k=1}^{k=N_Q} [[Q_k(j) - Q_k(i)]/\delta Q_k(j)]^2 \qquad (7)$$

where $\delta Q_k(j)$ is the error on Q_k. A best fit for the test model j is found by searching for the minimal χ^2_Q. Each point plotted is for a specific test model, that is classified only once. The scatter we see is between test-models, not the results of classifying one test model many times. The best fitting model is selected by performing a weighted average of those models that have $\chi^2 \leq 2 \times \chi^2_{MIN}$. The results are: errors of order 12% in temperature and 1 dex for $log(g)$ and $[Fe/H]$. However, a significant fraction of the scatter is correlated in the sense that metal-poor and metal-rich test models will have slightly different biases in the $log(g)$ classification. Likewise, $log(g)$-groups behave similarly in the $[Fe/H]$ classification.

In fact, the minimal norm method is not an optimal Q-classification scheme as some Q's contribute little and some Q's contribute a lot to the classification results. However, identifying the exact Q's to use for optimal classification is labor-intensive as it requires detailed investigation of many sub-groups of stars. Furthermore, extinction-free indices are not optimal classifiers for two reasons: 1) they assume a given R_V value, and 2) because four bands are used for each Q, the errors are approximately twice larger than the individual color measurements.

4.3. Color Classifiers

A more direct approach to the 3D classification of stars employs a χ^2 comparison of "observed" and model colors $(m_1 - m_2, m_1 - m_3, m_1 - m_4, ..., m_6 - m_7)$. Again, this is may not be an optimal method as some colors are better suited in certain regions of parameters space than others, as we saw in the case of metallicity dependent color gradients (fig. 6, left-hand panel). However, the advantage of the color-χ^2 minimization is that the extinction *amount* **and** R_V can be fitted directly. I have tested this approach by extending the computation of χ^2_C over a range of possible extinction and R_V values:

$$\chi^2_C(j; A_V, R_V) \;=\; \Delta||\overline{C}(j; A_V, R_V)|| = \sum_{i=1}^{i=15,937} \sum_{k=1}^{k=N_C} [[C_k(j) - C_k(i; A_V, R_V)]/\delta C_k(j)]^2 \qquad (8)$$

for all $N_C = 24$ colors, all A_V's and all R_V's tried. That is to say, each test model is compared with all 16k model atmospheres, where all training models are reddened by various A_V's and R_V's. As it turns out, effective temperature and extinction and R_V can be determined to 10%, 0.15 mag and 3%. The gravity and metallicity results are significantly better than for the $\overline{Q}$ classification, but still only moderately satisfactory. Note that the accuracy of the extinction determination is almost independent of A_V. As a result, extinction can be determined accurately towards highly reddened stars such as the Galactic Cepheids with $< A_V > \sim 1.5$ mag), but not so well for low-A_V sight-lines.

The 4-filter SDSS classification results are very comparable to the 8-band results, for all parameters. This is an indication of the limitation of the classification procedures followed in this memo. First, as mentioned above, the 4 SDSS filters only yield *three* independent colors so that it is *impossible* to determine all *five* parameters. The largest variation in the χ^2 values is due to T_{eff} and extinction, so that these parameters are well determined.

Blind χ^2 fitting as I have performed above is not necessarily optimal for determining the best fitting function. For example, suppose that one tries to fit a function to a noisy profile plus baseline. Each noisy baseline point will add approximately unity to χ^2, whatever the parameters of the function. Thus, incorporating more baseline points will tend to make the χ^2 minimum more shallow: little χ^2 variation can mean that too many points are included that carry little or no information on the parameters that are to be determined.

4.4. "Flux" Classifiers

I have tested the hypothesis that many of the 24 colors used in the previous subsection do not carry significant classification information. To this end I only used the "observed" fluxes in each of the 8 bands. However, each "flux" has to is normalized (by the i' band value), so that only 7 non-zero values remain. The resulting $\overline{F}$ classification scheme is identical to eqn. (8) but with $N_C = 7$ and $C_{k \neq i'} = m_k - i'$. The flux-classification scheme uses the data in the most direct manner, and produces results with the least amount of scatter. This result indicates that indeed many color-color (and $Q-Q$) combinations doe not contribute towards the classification of stellar spectra.

The flux-classification method shows that effective temperature can be determined to $\pm 3.5\%$, A_V to ± 60 mmag (6% for $A_V = 1$), R_V to $\pm 1.5\%$ and $log(g)$ and $[Fe/H]$ to 0.6 and 0.5 dex, respectively. Our results are about twice worse than those obtained by Bailer-Jones (2000) for the 11-band GAIA system. Note that Bailer-Jones did not attempt to determine the extinction parameters.

To some readers the extinction determination may sound to good to be true. Most

3D classification & extinction results reported in the literature are based on Strömgren photometry. However, remember that our 8-band system extends much further to the red (900 nm) than the Strömgren system (550 nm). As a result, ours and the Strömgren system cover factors three and 1.8 in extinction ratio. Thus our system has much more leverage to determine A_V and R_V (cf. fig. 1). As mentioned several times before, the *amount* of extinction is determined with constant accuracy in the 8-band system ($\pm$60 mmag). However, R_V is determines to 1-3%, independent of the value of A_V. Extinction parameters may be still better determined if external surveys such as 2MASS (near-infrared) and GALEX (near UV) can be included.

4.5. "Mixed" Classifiers

Finally, in order to make better use of the astrophysical information contained in the flux differences [Balmer jump $\leftrightarrow$ (u'-F422); Mg b $\leftrightarrow$ (g'-F520); TiO $\leftrightarrow$ (i'-F745); Paschen jump and Ca II triplet $\leftrightarrow$ (i'-F875)], I performed a χ^2 classification where I use all 7 independent fluxes *plus* the 7 adjacent-band colors. This scheme works better than the Flux classification, and I present the results in figure 7. From top to bottom, the results are for $T_{eff}, A_V, R_V, log(g)$ and $[Fe/H]$. In each panel, I plot results for four different temperature ranges.

The expected errors for FAME 8-band photometry is of order 10 mmag, at V=15. Figures 3-5 show that the $log(g)$ effects are of order several times the expected errors for most but not all bands. Thus, an increase of the errors could substantially reduce the classification results. Likewise, smaller errors would likely lead to much better classification results. The magnitude-effect is illustrated in figure 8. The five panels within each figure are for $T_{eff}, A_V, R_V, log(g)$ and $[Fe/H]$. Each curve represents results for a slightly different incarnation of the proposed 8-band filter system, where I experimented with increasing the bandwidths of the narrowest components, replacing u' with a slightly bluer set so as to increase the average throughput, by discarding the TiO_C band and replacing it with the z' band. As can be seen from these plots, the results are quite robust towards filter configuration. However, dumping the "UV" band altogether may have serious (TBD) consequences.

Inspection of these curves shows that 3D spectral classification employing intermediate band filters works extremely well, certainly at the bright end. Also note that all parameters but the gravity are better determined at low temperatures. Presumably, this is due to the fact that low temperature stars have more lines in their spectra, thereby facilitating their classification.

The discussion above indicates that optimal classification results can only be obtained

by careful selection of the bands that are to be included in the analysis. A sophisticated classification requires that different (combinations of) colors are used for different parts of parameters space. In this memo I have only touched upon this procedure. As Bailer-Jones (2000) showed, neural-network techniques can provide the required degree of non-linearity between the inputs (observed colors) and the outputs (stellar and inter-stellar physical conditions). Application of the more conventional $Q - Q$-diagrams can also be considered, and preliminary results suggest that a precision of 0.2-0.6 dex might be reachable.

5. Photometric Filters as ND Filters?

An average bandwidth of 100 nm corresponds to about 18% of the width of the astrometric CCDs and can thus observe stars of up to 1.9 magnitudes brighter without saturation. We could thus consider replacing the three neutral density filters that cover the magnitude range 7-9 with the 8-band filters. However, from the astrometric point of view, this is not a desirable situation as it increases the complexity of the calibration too much. However, it would be feasible to replace all ND filters of the same attenuation by *one* photometric filter. Ideally, these filters should be placed in a part of the spectrum where there are few lines, so that the astrometry is least affected by spectral characteristics of the stars.

From the photometric point of view, u', TiO_C and Ca II photometry have most to gain from an increased CCD area, as they have worst photometric errors. However, the number of photons in these bands depend substantially on T_{eff} as can be inferred from figure 6, and are thus a sub-optimal astrometric filters. In fact, the SED of a 3,500K star yields 1/53 (6) [12] times more photons in the u' (TiO_C) [CaII] band than a 30,000K star.

As a result of considering stars of a given apparent magnitude in the V band, there is *no* SED-induced variation in V. Thus, bands close to V have least SED-induced photon-number variations. For example, with respect to the 400-900 nm astrometric bandpass, the g', Mgb and r' bands have an attenuations of: (minimum, mean and maximum) = (0.69, 1.0, 1.72), (1.9, 2.1, 2.5), and (0.52, 1.1, 1.4) magnitudes. Further, the SED-induced variation in the astrometric bandpass (-0.74, -0.16, 0.0) is slightly larger than in the Mgb filter.

Stars of different spectral type would saturate the Mgb filter at different magnitudes: at V=7.1, V=6.9, V=6.9 and V=6.5 for B0, F7, G2 and M2 stars, respectively. Thus, the Mgb filter could replace the 1^{st} ND filter, which saturates at V=7. Likewise, for the TiO_C filter the saturation magnitudes are: V=5.3, V=6.0, V=6.2 and V=7.2 for B0, F7, G2 and M2 stars, respectively. Note that the actual saturation magnitudes are likely to be brighter since the PSFs of the actual FAME may very well be wider than assumed here (Monet, private communications).

Narrow filters have the nice property that they have virtually no spectra-type dependence of the PSF. For bright-star astrometry this is particularly important since the number of bright stars of a given color is rather small. Using the Mgb and TiO_C filters, the PSF can be constructed from bright-stars of *all* colors. If start-stop is not implemented, it will be crucial to use narrow-band filters for bright-star astrometry.

6. Discussion & Conclusions

Our T_{eff} results compare well to the those reported by Bailer-Jones (2000) for the GAIA photometric system. However, our gravity and metallicity classification results (0.4-1 dex) are significantly worse than for the GAIA system (0.2 dex), for most temperature ranges. Nevertheless the current methodology yields $log(g)$ errors that allow the distinction between main-sequence stars, subgiants, giants and supergiants. Also, with metallicity below 0.4 (0.7) dex for stars cooler than 7,000 (10,500) K, a good differentiation is possible between halo and Pop I objects, and between dwarfs and subdwarfs.

- The proposed 8-band photometric system is capable of determining effective temperature to 2-5%
- A_V to 60 mmag and R_V to 0.5-2%
- Metallicity and surface gravity are determined to 0.4-0.8 dex Mostly limited by: lack of blue photons and modeling difficulties
- Factor two improvement may be possible [e.g., neural-networks (Bailer-Jones 2000)]
- The photometric accuracies of the 8-band system are about 10.5 mmag or twice worse than that of the 4-band SDSS system.
- The 4-band SDSS system can only determine 3 parameters, and their results will be correlated with the parameters that are not determined.
- The various incarnations of 8-band systems have similar classification performance
- Astrometry in a 8-band photometric system will be unaffected, if not improved.
- The 8-band filter set has a transmittance comparable to that of the three V=7-9 neutral density filters. These chips could be used for other purposes: photometry, astrometry of bright targets, ...
- Classification results scale approximately linearly with photometric errors
- Astrometric accuracy is proportional to $FWHM_{PSF}^{3/2}$
- Photometric accuracy is independent of $FWHM_{PSF}$, to 1^{st} order

REFERENCES

Bailer-Jones, 2000, astro-ph/0003071

Cardelli J.A., Clayton G.C., Mathis J.S., 1989, ApJ, 345, 245

Fry A.M. & Carney B.W., 1997, AJ, 113, 1073

Jordi C., Masana E., Figueras F., Torra J., 1997, A&AS, 123, 1997

Le Jeune Th., Cuisinier F., Buser R., 1997, A&AS, 125, 229

McClure R. D. & van den Bergh S., 1968, AJ, 73, 313

Mihalas D., Binney J., 1981, Galactic Astronomy, W.H. Freeman and Company, San Francisco

Straižys, V. & Sviderskiene Z., 1972, A&A, 17, 312

Table 2: Astrometric and Photometric results for the astrometric CCDs as a function of visual magnitude (1^{th} column) or equivalently, peak flux (2^{nd} column) or signal-to-noise ratio (3^{rd} column). The photometric accuracy is tabulated in the last column. The single-observation astrometric error in column # 4, and the mission-equivalent errors in # 5. The values between brackets denote the theoretical attainable limit for a 2.5 year mission with 1059 statistically independent observations. Note that only half that many observations are taken per coordinate. The peak and total flux for V=9 star of the marginalized distribution are assumed to be: 602k and 950K electrons in the 400-900 nm band, and 52k and 316k in the 550-850 nm band (4700 e^- at V=14). The full widths at half maximum (FWHM) of the *optical PSF (Gaussian assumed)* in the in-scan and cross-scan directions are 1.41 and 5.65 pixels, respectively. In addition, a pill-box-like in-scan smear of 1.45 pixels is assumed (due to TDI mismatch). The simulations are the results of 50 random realizations that include Poisson & 12-electron read noise *per in-scan pixel* as well as digitization for each of 30 different sub-pixel locations. The values after the "slash" are calculated assuming a single-observation centroiding floor or $1/350^{th}$ of a pixel (values added in quadrature). Note that the astrometric accuracy decreases more rapidly than photon statistics below V=15, and gets really bad below V=17 or so. This is an undersampling effect: with about 50% of the flux in the central pixel, the S/N in the two next-brightest pixels is roughly half the S/N of the central pixel. At high flux levels, these results are somewhat overestimates due to the pixel-phase bias introduced by the 1.45-pill-box smearing.

V	Peak	S_{max}/N	$\delta x_0/\sqrt{\delta x_0^2 + 0.588^2}$	δx_0-mission	δm
mag	e^-		mas	mas	mmag
9.0	258828	508.6	0.318/0.618	(0.014/0.027)	1.69 (0.05)
10.0	102951	320.6	0.433/0.730	(0.019/0.032)	2.64 (0.08)
11.0	40939	201.9	0.599/0.840	(0.026/0.037)	4.08 (0.13)
12.0	16282	127.0	0.886/1.063	(0.038/0.046)	6.21 (0.19)
13.0	6473	79.5	1.498/1.610	(0.065/0.070)	10.31 (0.32)
14.0	2573	49.3	2.515/2.583	(0.109/0.112)	16.77 (0.52)
15.0	1022	29.9	4.533/4.571	(0.197/0.198)	30.11 (0.94)
16.0	408	17.3	8.642/8.662	(0.376/0.376)	57.22 (1.80)
17.0	167	9.4	18.105/18.11	(0.787/0.685)	116.8 (3.78)
18.0	79	5.2	44.625/44.63	(1.939/1.939)	225.7 (7.68)

Table 3: Astrometric and Photometric results for SDSS filters (FWHM=130 nm). For an explanation of the table's columns, see tab. 2. As each star will be observed by only one CCD, the number of independent observations equals 1059/14=75.6. The bracketed astrometric values are for 75.6/2=37.8 observations per coordinate, and the bracketed photometric errors are for 75.6 independent values.

V	Peak	S_{max}/N	δx_0	δm
mag	e^-		mas	mmag
9.0	119454	345.4	0.402 (0.065)	2.42 (0.28)
10.0	47498	217.6	0.554 (0.090)	3.80 (0.44)
11.0	18883	136.9	0.853 (0.139)	5.97 (0.69)
12.0	7506	85.8	1.383 (0.225)	9.51 (1.10)
13.0	2985	53.3	2.390 (0.389)	16.20 (1.87)
14.0	1186	32.5	4.137 (0.673)	26.99 (3.14)
15.0	473	18.9	7.689 (1.250)	49.89 (5.85)
16.0	192	10.4	15.943 (2.592)	103.39 (12.4)
17.0	85	5.6	37.776 (6.142)	205.63 (25.7)
18.0	42	3.1	102.37 (16.64)	357.67 (47.6)

Table 4: Astrometric and Photometric results for filters with a bandpass (FWHM=65 nm) that is *one-half* of the widths of the SDSS filters (8 filters total). For an explanation of the table's columns, see tab. 2. The bracketed astrometric errors are for 37.8/2 independent values, while 37.8 photometric observations can be used to obtain the misson-end average.

V	Peak	S_{max}/N	δx_0	δm
mag	e^-		mas	mmag
9.0	59680	244.0	0.51 (0.12)	3.22 (0.52)
10.0	23723	153.5	0.73 (0.17)	5.31 (0.87)
11.0	9428	96.3	1.21 (0.28)	8.50 (1.39)
12.0	3749	60.3	2.04 (0.47)	13.93 (2.28)
13.0	1490	36.8	3.59 (0.83)	23.27 (3.82)
14.0	593	21.8	6.57 (1.51)	43.10 (7.13)
15.0	230	12.2	13.36 (3.07)	84.31 (14.16)
16.0	104	6.5	30.58 (7.03)	176.42 (30.71)
17.0	49	3.5	78.71 (18.1)	318.31 (58.54)
18.0	25	1.9	156.74 (36.0)	460.36 (89.37)

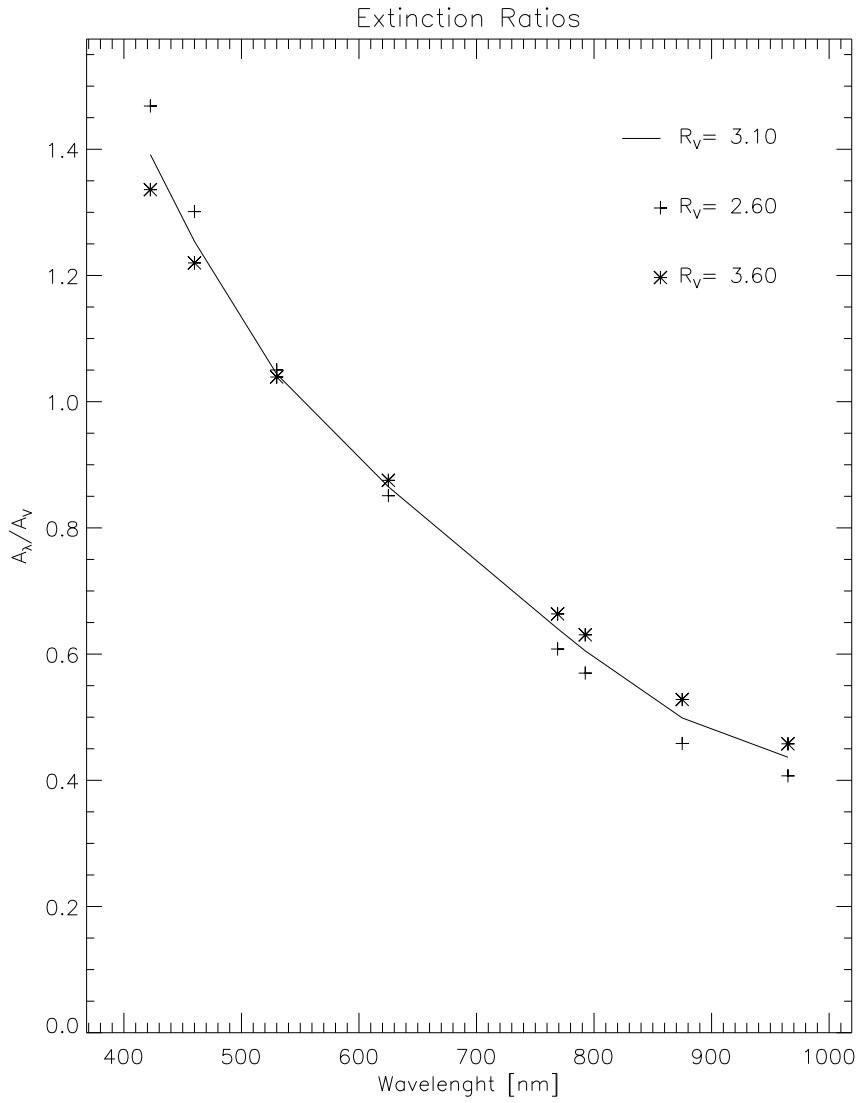

Fig. 1.— The extinction relative to the Johnson V band for the proposed 8-band filter system. The full line represents the "standard" $R_V = 3.1$ curve, the symbols are for slightly different R_V values. The extinction curve is determined according to the recipe of Cardelli, Clayton & Mathis (1989).

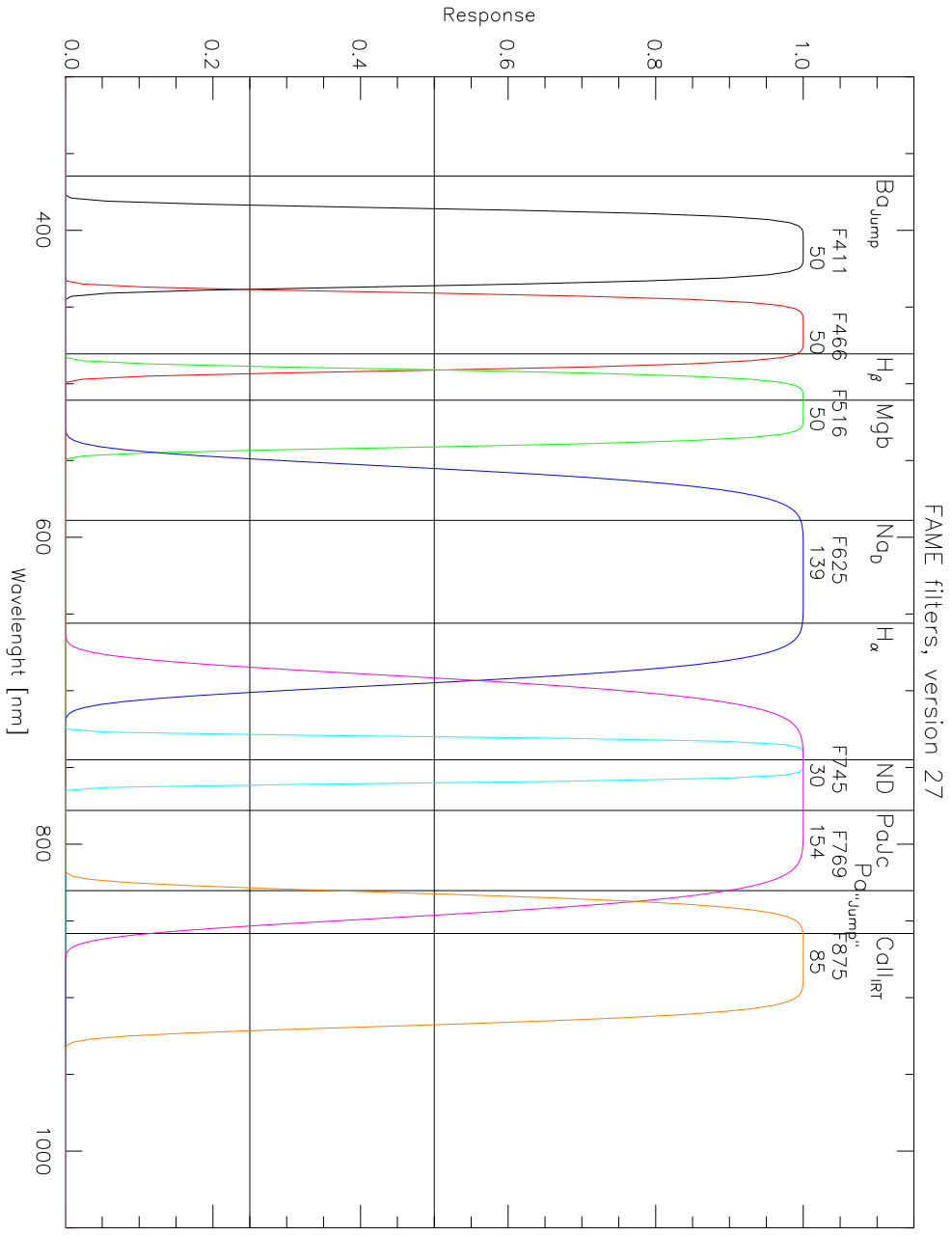

Fig. 2.— The proposed 8-band filter system. The central wavelengths and widths of the bands (in nm) are indicated above each band. The astrophysically interesting features discussed in the text are also indicated.

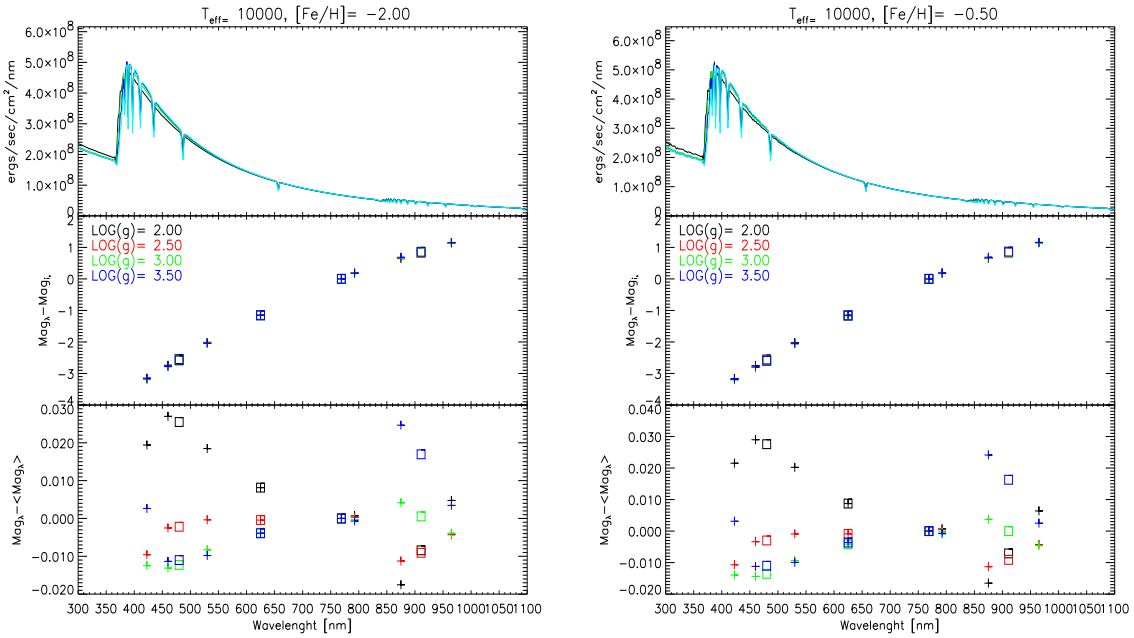

Fig. 3.— Top panels: model spectra for T_{eff} =10,000 K for several $log(g)$ values. Middle panels: intermediate-band fluxes normalized with respect to F769 (i'). The crosses mark members of the 8-band system, the boxes SDSS filters. Bottom panel: fluxes have been normalized with respect to the $log(g)$-averaged value. The left-hand set of plots are for a $[Fe/H]$=-2, the right-hand set for $[Fe/H] = -0.5$. Notice that metallicity has hardly any effect on the color differences.

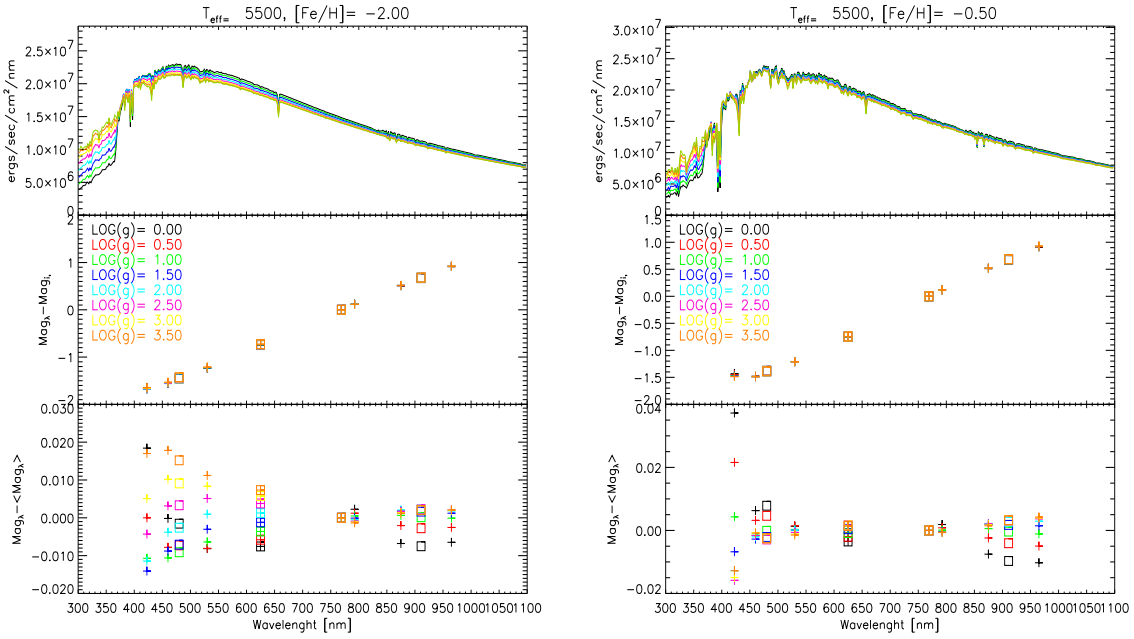

Fig. 4.— Same as for for figure 3, but for T_{eff}=5,500 K. The effects of the enhanced metallicity is rather subtle: The $log(g)$ color-variation for the bands blue-wards from i' (F769) is suppressed due to line-blanketing (lower panels).

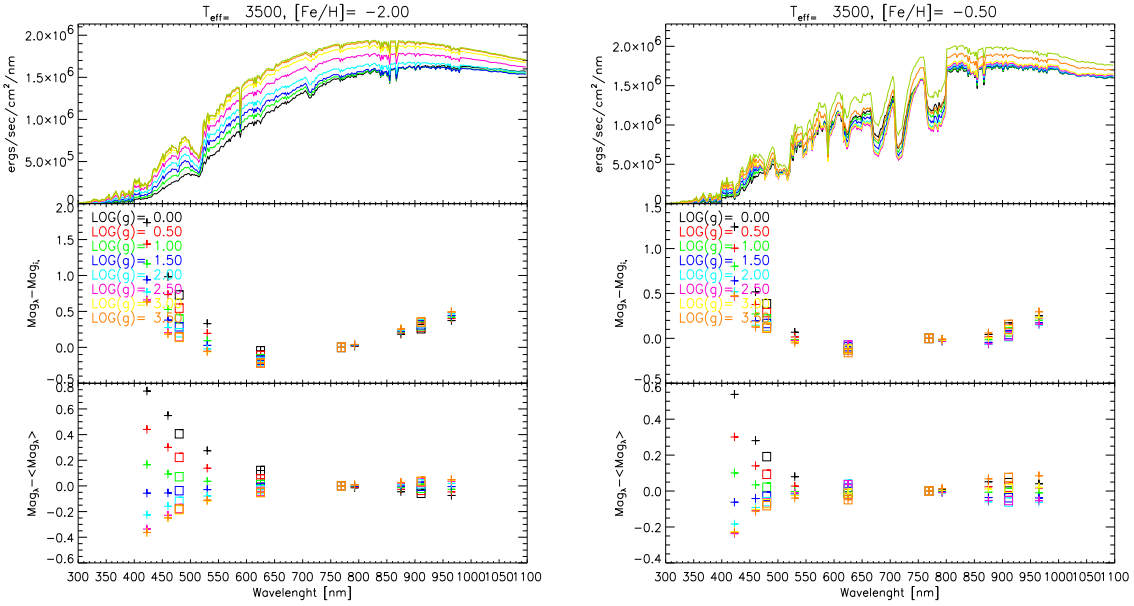

Fig. 5.— Same as for for figure 3, but for T_{eff}=3,500 K. For this temperature, metallicity effects show as a change of scale in the middle panels.

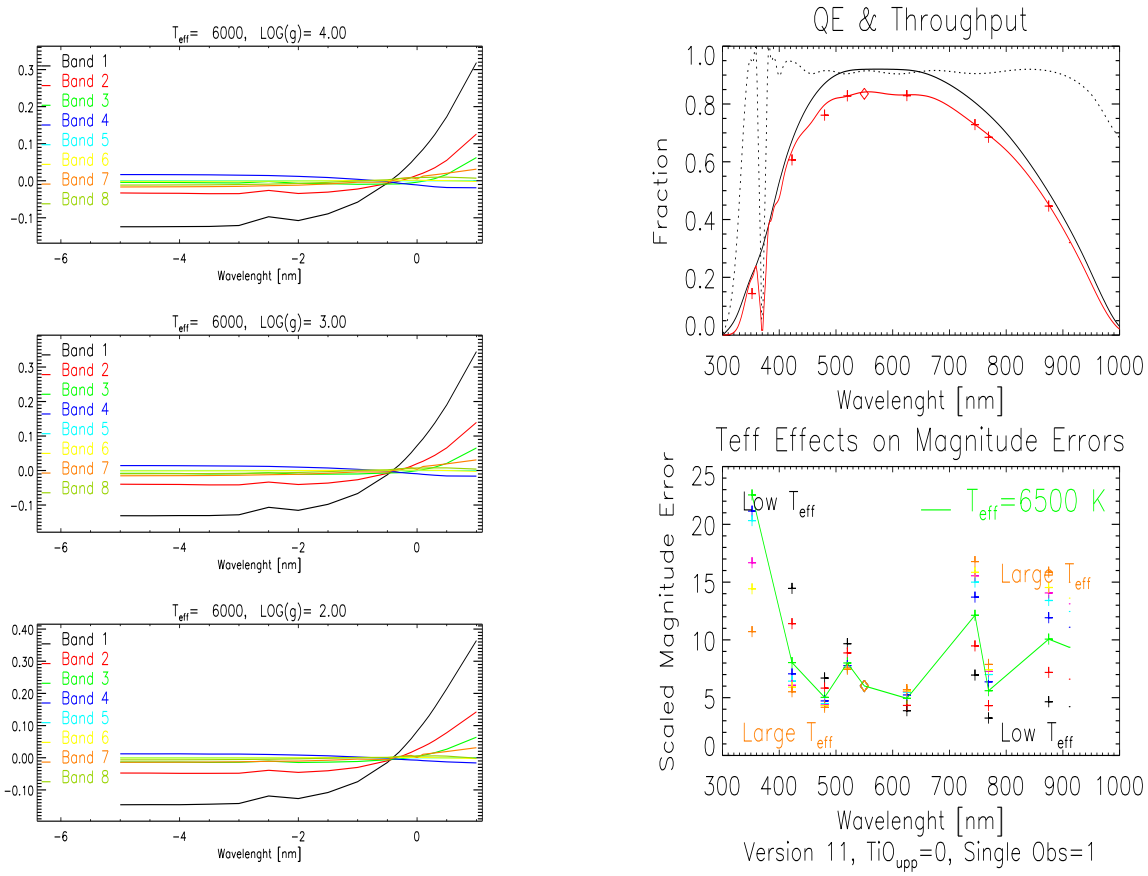

Fig. 6.— **Left-hand panel:** Metallicity variations in the 8-band system for G2-type stars. Main-sequence models are in the top figure [$log(g)$=4] and giant models in the lower two panels. It is clear that the bluest bands (1, 2 & 3) show the largest [Fe/H] gradients: the well-known line-blanketing in the blue (cf., the absorption features in fig. 4). The [Fe/H] gradients decrease from 100's of mmag in the blue to less than 10 mmag in the red. This figure illustrates the importance of reliable blue measurements. **Right-hand panel:** In the top panel I plot the quantum efficiency (full black line), optical throughput (dotted black line), and the product of the two (full red line). The crosses mark the central wavelengths of the 8-band filter set, the diamond the V band, and the dots the 4-band SDSS version. In the bottom panel I present the expect single-transit photometric errors for the 8-band filter set for "stars" with various T_{eff} values between 3,500 and 30,000 K. The T_{eff} = 6500K model is connect with the green line. Notice that for the u' band, the errors are larger than 25 mmag, for $T_{eff} \lesssim 7000$.

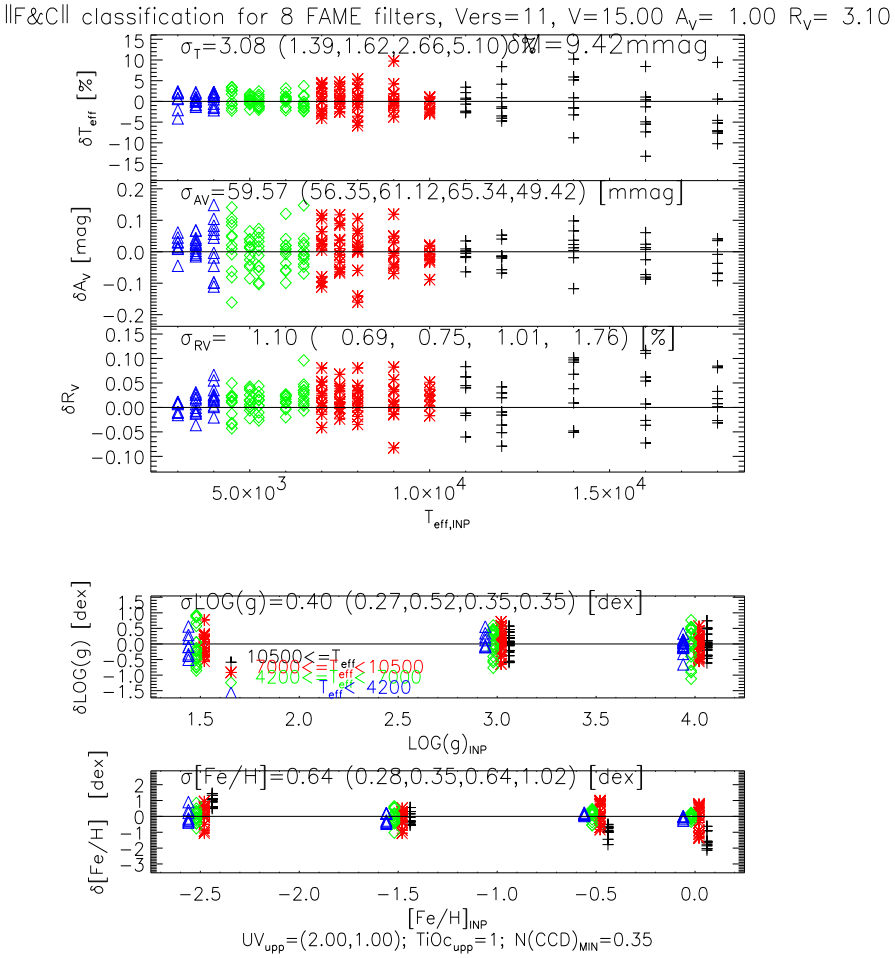

Fig. 7.— Minimal $||\overline{F\&C}||$ 3D classification results in the 8-band system. In each panel, four temperature ranges are indicated: 1) $T_{eff} < 4200$ (blue triangles), 2) $4200 \leq T_{eff} < 7000$ (green diamonds), 3) $7000 \leq T_{eff} < 10,500$ (red stars), and 4) $T_{eff} \geq 10,500$ (black crosses). The σ values listed are for the whole temperature range, the values in brackets for the temperature subsets mentioned above. In each panel, 5 RMS classification errors are listed: the 1^{th} for all temperatures, the values between brackets for the four temperature ranges (from low to high). Effective temperature, extinction and R_V are determined to great precision at V=15: 3%, 6% and 1% respectively. Surface gravity and metallicity have errors of 0.4 and 0.6 dex.

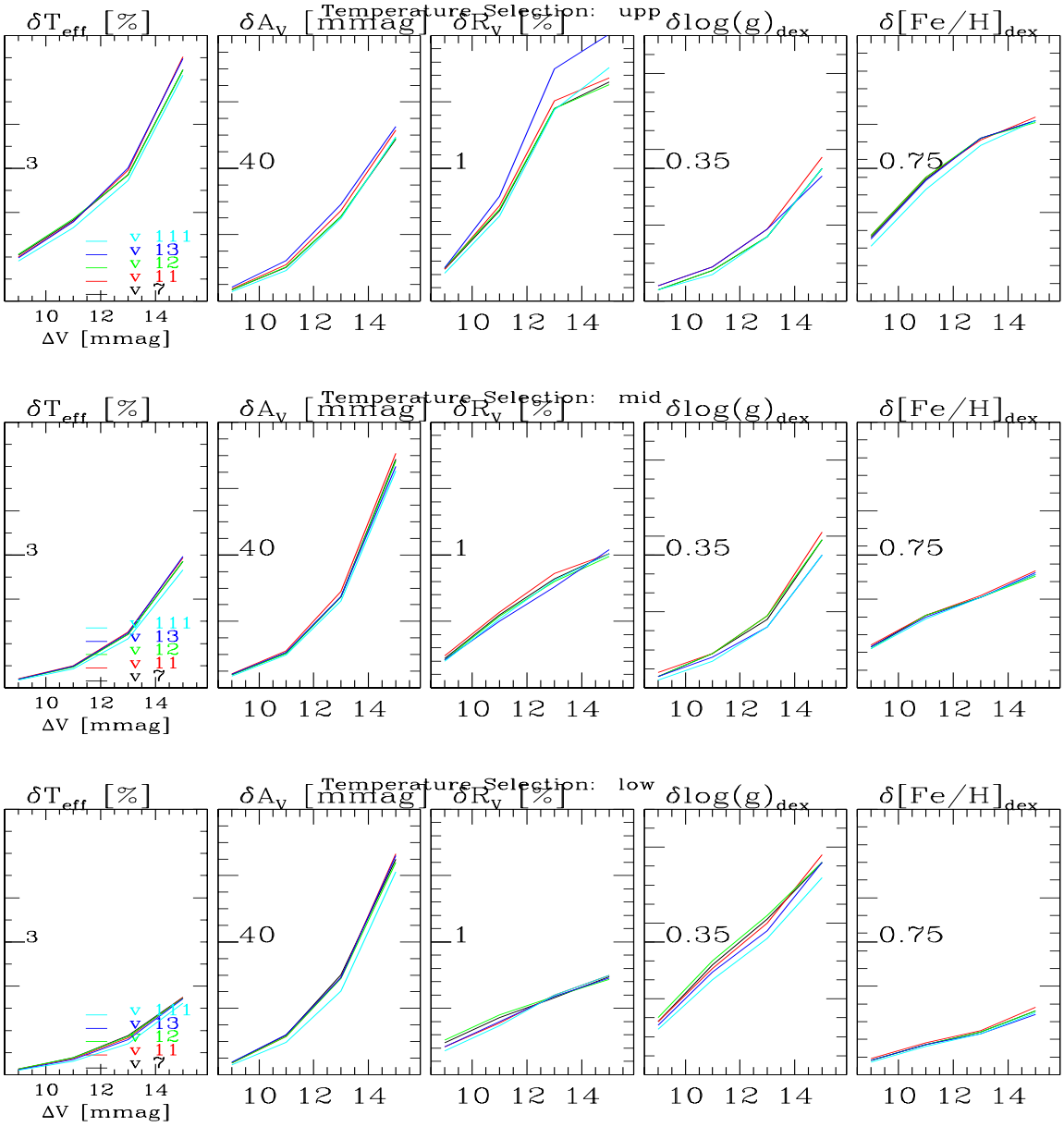

Fig. 8.— 3D classification results in the 8-band system as a function of apparent magnitude. In the three figures I present the classification results for, from bottom to top: 1) $4200 \leq T_{eff} < 7000$, 2) $7000 \leq T_{eff} < 10,500$, and 3) $T_{eff} \geq 10,500$. The five panels within each figure are for $T_{eff}, A_V, R_V, log(g)$ and $[Fe/H]$, from left to right. The *scale* is indicated inside each box by the tick-mark at half-maximum. Clearly, the classification errors depend approximately linearly on the in-band magnitude (errors).